

Supporting Information:

Raising thermoelectric performance of n-type SnSe  
via Br doping and Pb alloying

Cheng Chang,<sup>a</sup> Qing Tan,<sup>b</sup> Yanling Pei,<sup>a</sup> Yu Xiao,<sup>a</sup> Xiao Zhang,<sup>a</sup> Yue-Xing Chen,<sup>c</sup> Lei Zheng,<sup>a</sup> Shengkai Gong,<sup>a</sup> Jing-Feng Li,<sup>b</sup> Jiaqing He,<sup>c</sup> Li-Dong Zhao<sup>a,\*</sup>

<sup>a</sup>*School of Materials Science and Engineering, Beihang University, Beijing 100191, China*

<sup>b</sup>*School of Materials Science and Engineering, Tsinghua University, Beijing 100084, China*

<sup>c</sup>*Department of Physics, South University of Science and Technology of China, Shenzhen 518055, China*

\*Corresponding author: zhaolidong@buaa.edu.cn

**Experimental**

**Starting materials:** Sn chunk (99.999%, Aladdin, China), Se shot (99.999%, Aladdin, China), Pb shot (99.999%, Aladdin, China), SnBr<sub>2</sub> powder (99.2%, Alfa, US)

**Synthesis:** To prepare ingots (~10g) with nominal compositions of SnSe<sub>1-x</sub>Br<sub>x</sub> (x=0.01, 0.02, 0.03, 0.04) and Sn<sub>1-x</sub>Pb<sub>x</sub>Se<sub>0.97</sub>Br<sub>0.03</sub> (x=0.025, 0.05, 0.1, 0.2, 0.3), high purity raw materials were mixed with stoichiometric proportions into quartz tubes in a N<sub>2</sub>-filled glove box to prevent raw materials from reacting with air, especially SnBr<sub>2</sub>. Then the tube was evacuated to a pressure of 10<sup>-4</sup> torr, flame-sealed, then placed it into another bigger quartz tube, evacuated and flame-sealed again. The outer tube is used to prevent the crystal from oxidation by air, because the inner tube breaks when cooling to room temperature owing to the considerable difference of thermal expansion between the crystal and quartz. The tubes were slowly heated to 1223 K in 9 h, then soaked at this temperature for 6 h and subsequently air quenched to room temperature. The obtained ingots were grounded into powder of ~100 mesh with agate mortar in a N<sub>2</sub>-filled glove box and then densified by spark plasma sintering (SPS-211Lx) in a  $\Phi$  12.7 mm graphite die at 793K under an axial pressure of 50MPa. Finally, cylinder-shaped samples with high relative density of >97% were obtained.

**X-ray diffraction:** The powder samples were prepared by grinding ingots in an agate mortar. The XRD patterns were performed on a Rigaku (D-Max 2500) instrument with Cu K <sub>$\alpha$</sub>  ( $\lambda=1.5418\text{\AA}$ ) radiation and a step size of 0.02°.

**Electrical properties:** The obtained SPS processed pellets were cut along the direction perpendicular and parallel to the SPS pressure direction respectively and polished to bars with dimensions of ~11 mm  $\times$  3 mm  $\times$  3 mm. The electrical transport property measurements were performed with an Ulvac Riko ZEM-3 instrument which can measure the Seebeck coefficient and the electrical conductivity simultaneously. Before measurement, the samples were coated with a thin layer of boron nitride (BN) to protect instrument. The uncertainty of the Seebeck coefficient and electrical conductivity measurements is 5%.

**Thermal conductivity:** The SPS processed pellets were cut into coins with dimension of  $\Phi$  ~ 6 mm  $\times$  1.5 mm along the direction perpendicular and parallel to the SPS pressure direction respectively. The thermal diffusivity were measured with a

Netzsch LFA 457 instrument and analyzed using a Cowan model with pulse correction. To minimize the error induced by the emissivity of the material, the coins were well polished and coated with a thin layer of graphite. The thermal conductivity were calculated *via*  $\kappa = \alpha \cdot C_p \cdot \rho$ , where  $\alpha$ ,  $C_p$ ,  $\rho$  are thermal diffusivity, specific capacity and density, respectively. The specific heat capacity ( $C_p$ ) was taken from reference.<sup>1,2</sup> The density ( $\rho$ ) was determined using the dimensions and mass of the sample, shown in Table S1. The uncertainty of the thermal conductivity is estimated to be within 5%, considering the uncertainties for  $D$ ,  $C_p$  and  $\rho$ . The combined uncertainty for all measurements involved in the calculation of  $ZT$  is about 20 %.

**Hall coefficient measurement:** Hall coefficient ( $R_H$ ) was measured under a reversible magnetic field (0.8 T) by the Van der Pauw method by using a Hall measurement system (Lake Shore 8400 Series, Model 8404, USA). Carrier density ( $n_H$ ) was obtained by  $n_H = 1/(eR_H)$ , and carrier mobility ( $\mu_H$ ) was calculated by  $\mu_H = \sigma R_H$ .

**Lorenz number calculation:**

The Lorenz number is given by formula<sup>3</sup>

$$L = \left( \frac{k_B}{e} \right) \left( \frac{(r + 7/2)F_{r+5/2}(\eta)}{(r + 3/2)F_{r+1/2}(\eta)} \right) - \left[ \frac{(r + 5/2)F_{r+3/2}(\eta)}{(r + 3/2)F_{r+1/2}(\eta)} \right]^2 \quad (\text{S1})$$

where  $k_B$  is the Boltzmann constant and  $\eta$  represents the reduced Fermi energy, which can be derived from the measured Seebeck coefficients *via* the following equation

$$S = \pm \frac{k_B}{e} \left( \frac{(r + 5/2)F_{r+3/2}(\eta)}{(r + 3/2)F_{r+1/2}(\eta)} - \eta \right) \quad (\text{S2})$$

where  $F_n(\eta)$  is the  $n$ th order Fermi integral:

$$F_n(\eta) = \int_0^\infty \frac{\chi^n}{1 + e^{\chi - \eta}} d\chi \quad (\text{S3})$$

$$\eta = \frac{E_f}{k_B T} \quad (\text{S4})$$

Acoustic phonon scattering has been assumed as the main carrier scattering mechanism, resulting in  $r$  value of  $-1/2$ .<sup>4</sup>

**Table S1.** Nominal compositions, sample densities, carrier concentrations and carrier mobilities of  $\text{SnSe}_{1-x}\text{Br}_x$  ( $x=0\sim 0.04$ ) and  $\text{Sn}_{1-x}\text{Pb}_x\text{Se}_{0.97}\text{Br}_{0.03}$  ( $x=0\sim 0.3$ ).

Nominal composition	Density( $\text{g cm}^{-3}$ )	$n_{\text{H}}$ ( $10^{17}\text{cm}^{-3}$ )	$\mu_{\text{H}}$ ( $\text{cm}^2\text{V}^{-1}\text{s}^{-1}$ )
SnSe	5.80	2.25	12.5
$\text{SnSe}_{0.99}\text{Br}_{0.01}$	5.78	0.48	0.43
$\text{SnSe}_{0.98}\text{Br}_{0.02}$	5.78	0.59	0.87
$\text{SnSe}_{0.97}\text{Br}_{0.03}$	5.80	18.3	0.6
$\text{SnSe}_{0.96}\text{Br}_{0.04}$	5.94	102	0.32
$\text{Sn}_{0.975}\text{Pb}_{0.025}\text{Se}_{0.97}\text{Br}_{0.03}$	5.81	33.1	0.6
$\text{Sn}_{0.95}\text{Pb}_{0.05}\text{Se}_{0.97}\text{Br}_{0.03}$	5.88	6.57	0.14
$\text{Sn}_{0.9}\text{Pb}_{0.1}\text{Se}_{0.97}\text{Br}_{0.03}$	5.91	2.13	1.56
$\text{Sn}_{0.8}\text{Pb}_{0.2}\text{Se}_{0.97}\text{Br}_{0.03}$	6.11	54.8	0.63
$\text{Sn}_{0.7}\text{Pb}_{0.3}\text{Se}_{0.97}\text{Br}_{0.03}$	6.34	123	1.84

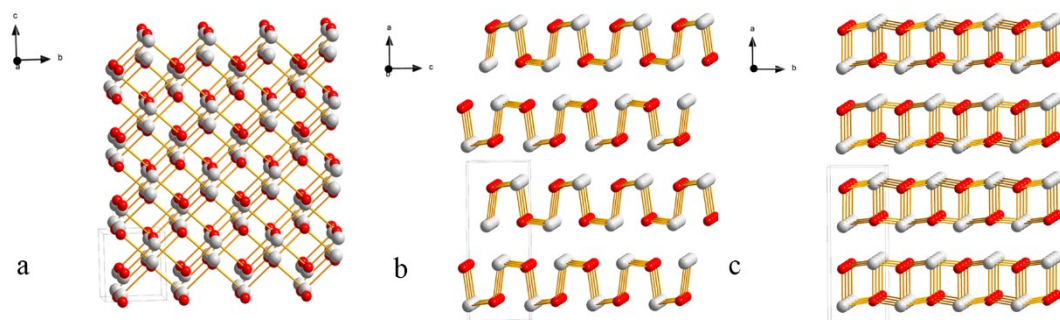


**Figure S1.** Crystal structure of SnSe along (a) the a-axis direction, (b) the b-axis direction, (c) the c-axis direction.

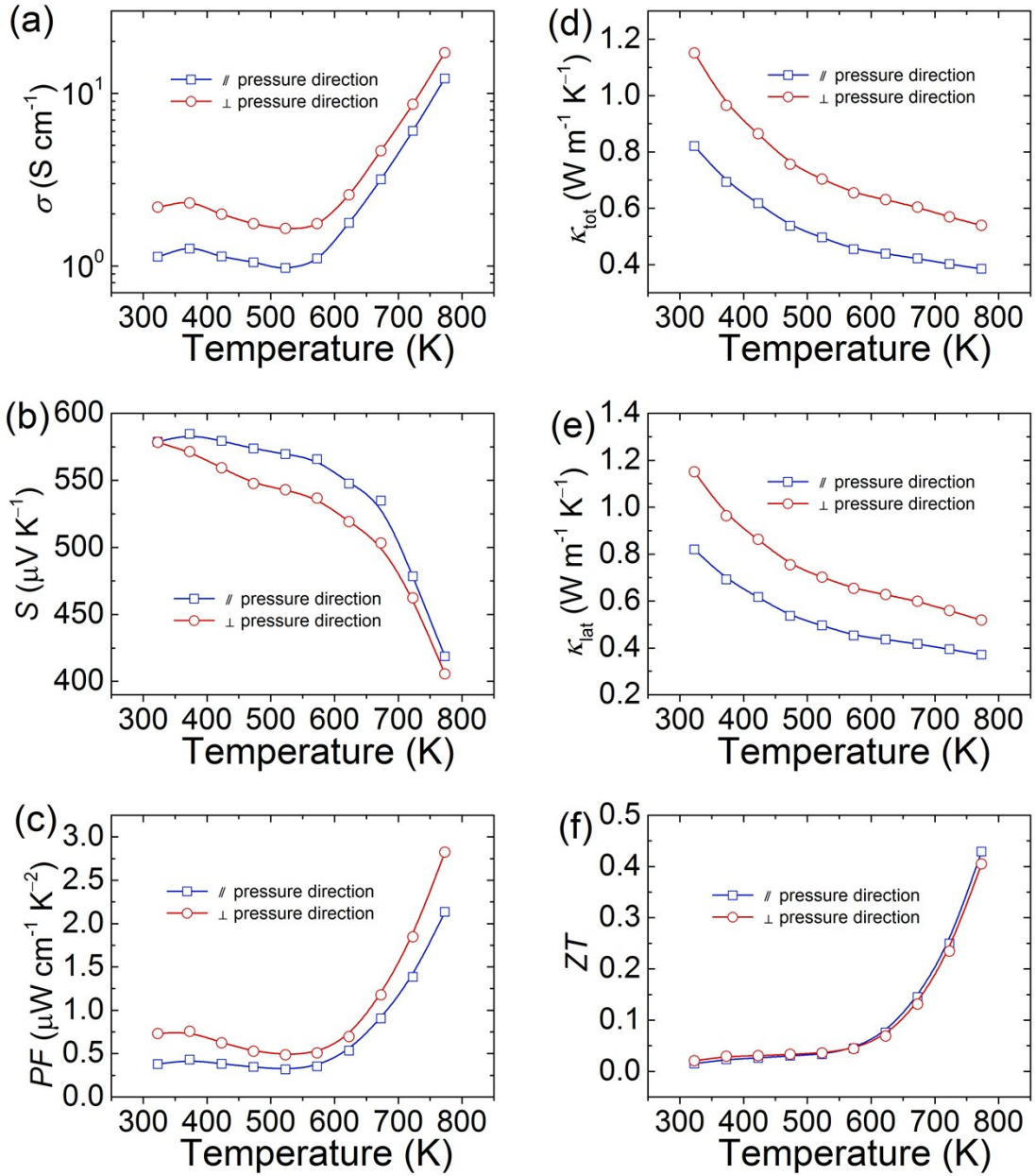


**Figure S2.** Temperature dependence of a) electrical conductivity, b) Seebeck coefficient, c) power factor, d) total thermal conductivity, e) lattice thermal conductivity, and f)  $ZT$  for undoped SnSe measured perpendicular and parallel to the pressing direction.

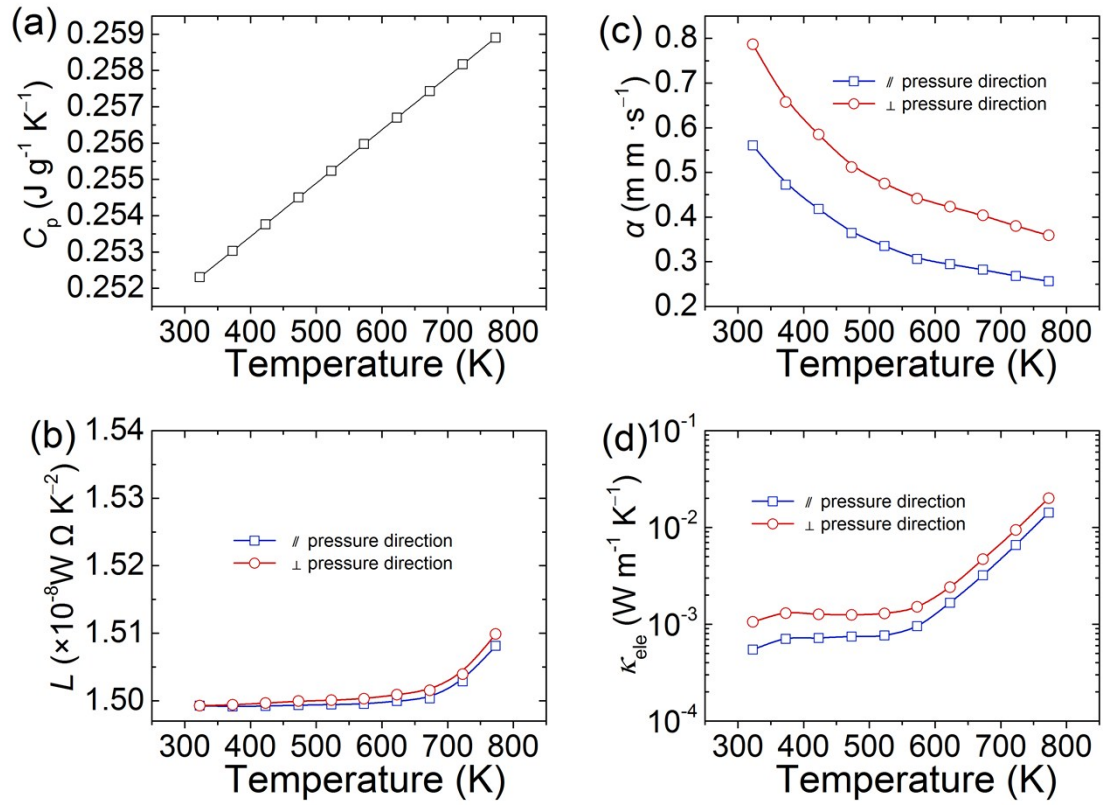


**Figure S3.** Temperature dependence of a) specific heat, b) Lorenz number, c) thermal diffusivity and d) electron thermal conductivity for SnSe measured perpendicular and parallel to the SPS pressing direction.

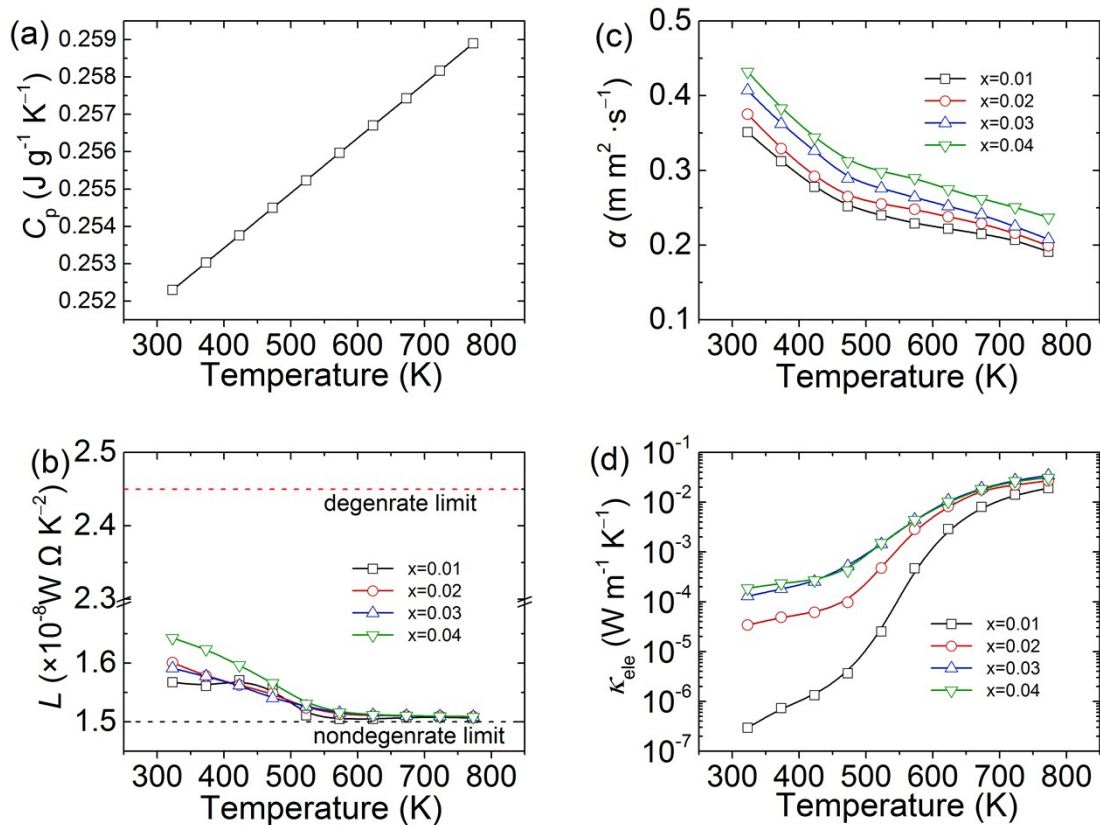


**Figure S4.** Temperature dependence of a) specific heat, b) Lorenz number, c) thermal diffusivity and d) electron thermal conductivity for SnSe<sub>1-x</sub>Br<sub>x</sub> (  $x = 0, 0.01, 0.02, 0.03,$  and  $0.04$ ) measured along the direction parallel to the SPS pressing direction.

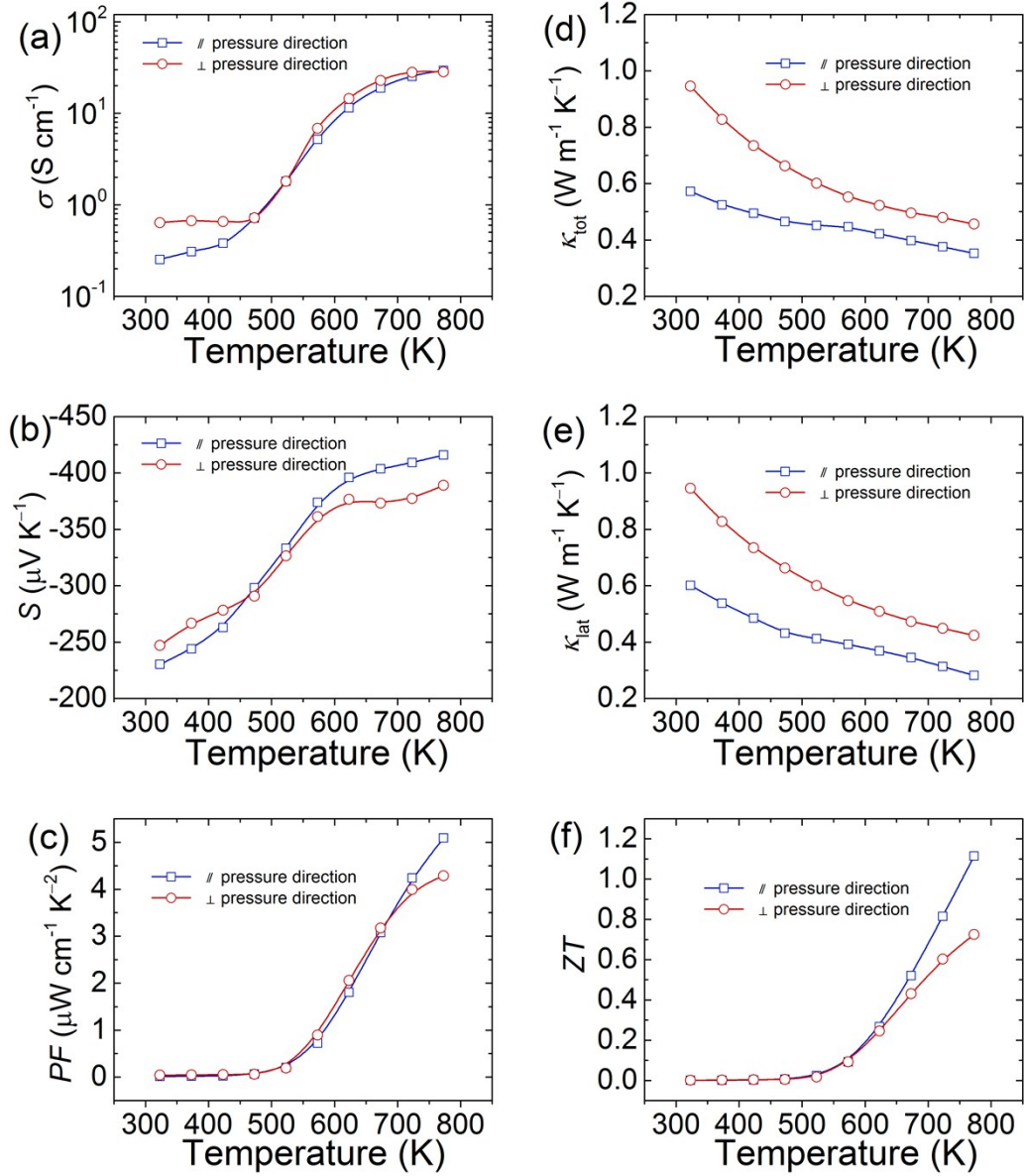


**Figure S5.** Temperature dependence of a) electrical conductivity, b) Seebeck coefficient, c) power factor, d) total thermal conductivity, e) lattice thermal conductivity, and f)  $ZT$  for  $\text{SnSe}_{0.97}\text{Br}_{0.03}$  measured along the directions perpendicular to and parallel to the SPS pressing direction.

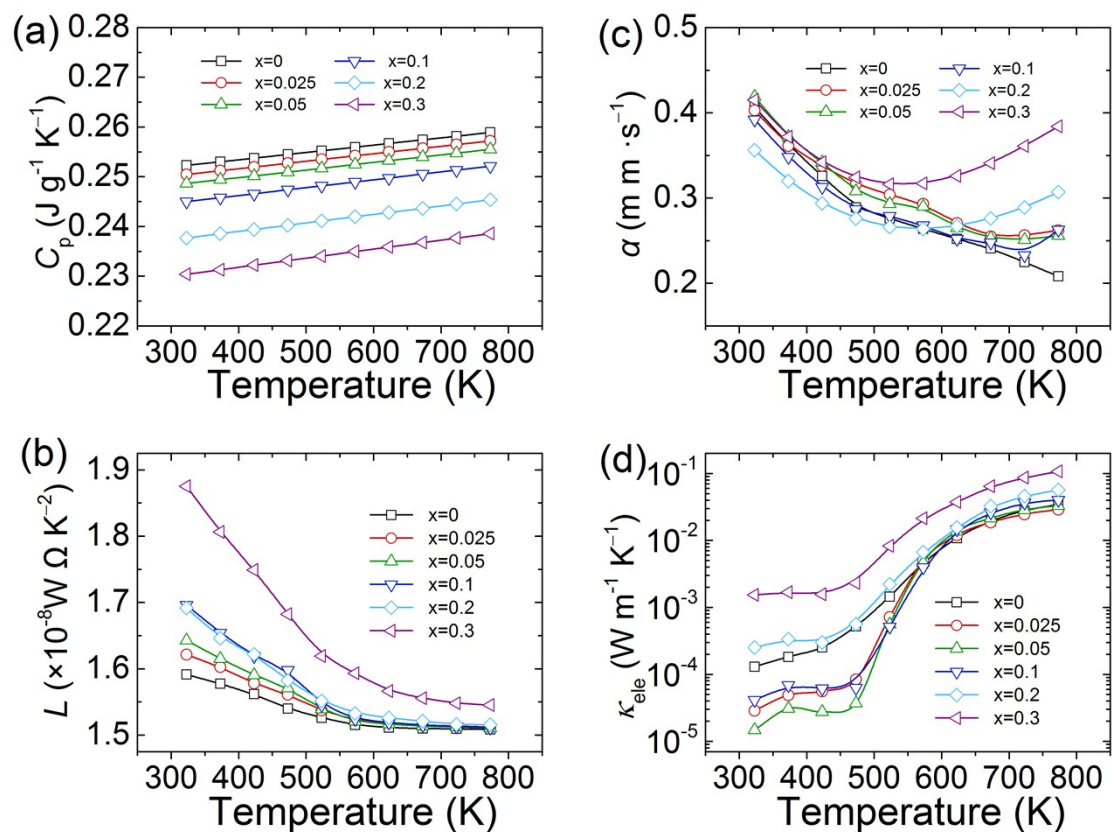


**Figure S6.** Temperature dependence of a) specific heat, b) Lorenz number, c) thermal diffusivity and d) electron thermal conductivity for  $\text{Sn}_{1-x}\text{Pb}_x\text{Se}_{0.97}\text{Br}_{0.03}$  ( $x = 0 \sim 0.3$ ) measured along the direction parallel to the SPS pressing direction.

- (1) Wang, H.; Gibbs, Z. M.; Takagiwa, Y.; Snyder, G. J. *Energy & Environmental Science* **2014**, *7*, 804.
- (2) Zhao, L. D.; Lo, S. H.; Zhang, Y.; Sun, H.; Tan, G.; Uher, C.; Wolverton, C.; Dravid, V. P.; Kanatzidis, M. G. *Nature* **2014**, *508*, 373.
- (3) Liu, W.-S.; Zhang, Q.; Lan, Y.; Chen, S.; Yan, X.; Zhang, Q.; Wang, H.; Wang, D.; Chen, G.; Ren, Z. *Advanced Energy Materials* **2011**, *1*, 577.
- (4) Zhao, L. D.; Zhang, B. P.; Liu, W. S.; Zhang, H. L.; Li, J. F. *Journal of Alloys and Compounds* **2009**, *467*, 91.